https://doi.org/10.5194/acp-2020-495
Preprint. Discussion started: 29 June 2020

Atmospheric Chemistry and Physics Discussions

The response of stratospheric water vapor to climate change driven by different forcing agents

Xun Wang[1] and Andrew E. Dessler[1]

[1]Department of Atmospheric Sciences, Texas A&M University, College Station, TX, USA

Correspondence to: Andrew E. Dessler (adessler@tamu.edu)

Abstract. We investigate the response of stratospheric water vapor (SWV) to different forcing agents within the Precipitation Driver and Response Model Intercomparison Project (PDRMIP) framework. For each model and forcing agent, we break the SWV response into a slow response, which is coupled to surface temperature changes, and a fast SWV, which is the direct response to external forcing, but without any mediation from the surface temperature. Our results show that, for most climate perturbations, the slow SWV response dominates the fast response. The slow SWV response exhibits a similar sensitivity to surface temperature across all climate perturbations. Specifically, the sensitivity is 0.35 ppmv K^{-1} in the tropical lower stratosphere (TLS), 2.1 ppmv K^{-1} in the northern hemispheric lowermost stratosphere (LMS), and 0.97 ppmv K^{-1} in the southern hemispheric LMS. The fast SWV response only dominates the slow SWV response when the forcing agent radiatively heats the cold point region — for example, black carbon, which directly heats the atmosphere by absorbing solar radiation. The fast SWV response in the TLS is primarily controlled by the fast adjustment of cold point temperature across all climate perturbations. This control becomes weaker at higher altitudes and at higher latitudes below 150 hPa.

1 Introduction

Stratospheric water vapor plays an important role in global climate change. It is an important greenhouse gas (GHG), which affects the Earth's radiative budget (Forster and Shine, 2002; Solomon et al., 2010), and it also plays an important role in stratospheric ozone chemistry (Solomon et al., 1986; Dvortsov and Solomon, 2001).

SWV in the overworld (above 380-K isentropic surface) (e.g. Hoskins, 1991) and SWV in the extratropical lowermost stratosphere (LMS, between the extratropical tropopause and the 380-K isentropic surface) (e.g. Holton et al., 1995) are distinguished according to different mechanisms that control them. Overworld SWV is primarily controlled by the temperatures in the tropical tropopause layer (TTL) as air is transported through it (e.g. Mote et al., 1996; Fueglistaler et al., 2009) and by production from oxidation of methane (e.g. Brasseur and Solomon, 2005). The LMS SWV is controlled by three major sources, including the transport of overworld air by the downward branch of Brewer-Dobson circulation, adiabatic quasi-horizontal transport from the tropical upper troposphere, and diabatic cross-tropopause transport due to deep convection (Dessler et al., 1995; Holton et al., 1995; Plumb, 2002; Gettelman et al., 2011).

https://doi.org/10.5194/acp-2020-495
Preprint. Discussion started: 29 June 2020

The response of SWV to climate change can be partitioned into two components: the fast response and slow response. The addition of a radiatively active constituent to the atmosphere can influence the atmosphere even before the surface temperature changes, leading to changes in SWV. This is often referred to as an "adjustment" to the forcing, and is generally considered part of the external forcing (e.g. Sherwood et al., 2015). We will refer to this as the "fast response" of SWV to the forcing. The slow response is the component in the SWV change that is coupled to changes of the surface temperature, which occurs on longer time scales. This slow response means that SWV could be an important positive feedback to global warming (Forster and Shine, 2002; Dessler et al., 2013; Huang et al., 2016; Banerjee et al., 2019). Banerjee et al. (2019) have shown that, when CO_2 is abruptly quadrupled, the change in SWV mainly consists of the slow response and that the fast response is less important.

Previous studies have shown that climate models, which are able to accurately reproduce observed interannual variations in SWV (Dessler et al., 2013; Smalley et al., 2017), robustly project a positive long-term trend in overworld SWV at entry level with a warming climate due to increasing GHGs (Gettelman et al., 2010; Dessler et al., 2013; Smalley et al., 2017). This is mainly due to a warmer tropopause (Thuburn and Craig, 2002; Gettelman et al., 2010; Lin et al., 2017; Smalley et al., 2017; Xia et al., 2019), which is controlled, to some extent at least, by the warming surface (Gettelman et al., 2010; Shu et al., 2011; Dessler et al., 2013; Huang et al., 2016; Revell et al., 2016; Lin et al., 2017; Smalley et al., 2017; Banerjee et al., 2019). Dessler et al. (2016) suggested that increases in convective injection into the stratosphere due to a warming climate may also be contributing to the trend in entry SWV. In the LMS, the climate models show larger increases in SWV (Dessler et al., 2013; Huang et al., 2016; Banerjee et al., 2019). It is not known how SWV responses to different forcing agents.

The goal of this study is to investigate the response of both overworld and LMS SWV to forcing agents with different physical properties. We will explicitly investigate the fast and slow responses in SWV and compare them. We will also investigate how SWV responds to surface temperature change when the climate is forced by different forcing agents.

2. Method

2.1 The PDRMIP set-up

In this paper, we analyze nine models from the Precipitation Driver and Response Model Intercomparison Project (PDRMIP) (Samset et al., 2016; Myhre et al., 2017; Tang et al., 2018, 2019). These are Coupled Model Inter-comparison Project phase 5 (CMIP5) era models (Table 1) and each performed a baseline and multiple climate perturbation experiments (Table 1).

In the perturbation experiments, perturbations on a global scale are applied abruptly at the beginning of the model simulation. The five core experiments include a doubling of CO_2 concentration (2xCO_2), a tripling of CH_4 concentration (3xCH_4), a 2% increase in solar irradiance (2%Solar), an increase of present-day black carbon concentration or emission by

https://doi.org/10.5194/acp-2020-495
Preprint. Discussion started: 29 June 2020

Atmospheric Chemistry and Physics Discussions
Open Access

factor of 10 (10xBC), and an increase of present-day SO_4 concentration or emission by factor of 5 (5xSO_4). In addition to the five core experiments, a subset of models also performed additional perturbation experiments: an increase in CFC-11 concentration from 535 ppt to 5 ppb (hereafter, 10xCFC-11), an increase in CFC-12 concentration from 653.45 ppt to 5 ppb (hereafter, 10xCFC-12), an increase in N_2O concentration from 316 ppb to 1 ppm (hereafter, 3xN_2O), an increase tropospheric O_3 concentration used in MacIntosh et al. (2016) by factor of 5 (5xO_3), and an increase of present-day black carbon with shorter lifetime by factor of 10 (10xBCSLT). Table 1 provides details about the models and the perturbations each one simulated.

The perturbations in GHGs and solar irradiance are relative to the models' baseline simulations, in which the concentration of the GHGs and solar irradiance are either at present-day levels or pre-industrial levels. The perturbations in the aerosols depend on whether it is possible to prescribe aerosol concentrations in the models. For models that are able to prescribe aerosol concentrations, the aerosol perturbations are based on a multi-model mean baseline aerosol concentration in 2000 obtained from the AeroCom Phase II initiative (Myhre et al., 2013). For those that are only able to produce aerosols through emissions, the perturbation is applied by increasing the emissions by the factors listed above. The 10xBCSLT experiment is performed only by models that are able to prescribe aerosol concentrations.

Each perturbation experiment is performed in two configurations: a fixed sea surface temperatures simulation ("fixed SST") and a fully coupled (slab ocean for CAM4 only) simulation. The fixed SST simulations use the SST climatology at either present-day level or pre-industrial level. The fixed SST simulations are at least 15 years and the coupled simulations are at least 100 years.

2.2 Fast response and slow response

When available, SWV mixing ratio is obtained directly from the specific humidity output by each model simulation. For the models that do not output specific humidity (CAM5, GISS-E2-R, and MIROC-SPRINTARS), we calculate specific humidity by multiplying the models' relative humidity by the saturation mixing ratio with respect to ice calculated using model temperature and pressure.

We define ΔSWV, the change in SWV mixing ratio in response to a particular perturbation, to be the difference between SWV in the perturbed coupled run and that in the baseline coupled run. As discussed above, the ΔSWV can then be broken down into the two components: the fast response (ΔSWV_{fast}) and slow response (ΔSWV_{slow}). We compute results in the tropical lower stratosphere (70 hPa, 30°N-30°S, hereafter, TLS), in the northern hemispheric (NH) lowermost stratosphere (50°N-90°N at 200 hPa, hereafter, NH LMS), and in the southern hemispheric (SH) lowermost stratosphere (50°S-90°S at 200 hPa, hereafter, SH LMS). Most previous studies have focused on response of water vapor in the TLS (e.g., Gettelman et

https://doi.org/10.5194/acp-2020-495
Preprint. Discussion started: 29 June 2020

al., 2010; Shu et al., 2011; Smalley et al., 2017). But recent studies report that the climate is most sensitive to changes in water vapor in the LMS (Solomon et al., 2010; Dessler et al., 2013; Banerjee et al., 2019), so we also investigate that region.

We use the fixed SST simulations to get ΔSWV_{fast}, the change in SWV before the surface temperature changes. ΔSWV_{fast} is the difference between the SWV mixing ratio averaged over the last 10 years in the fixed SST run with the forcing perturbation and the SWV mixing ratio averaged over the last 10 years in the fixed SST run with the baseline atmosphere.

We calculate ΔSWV_{slow} as ΔSWV minus ΔSWV_{fast}. To estimate the time series of ΔSWV_{slow}, we use annual mean ΔSWV over the entire coupled run period (at least 100 years) minus the ten-year average ΔSWV_{fast}. To estimate equilibrium ΔSWV_{slow}, we use a regression method similar to the methodology introduced by Gregory et al. (2004). The basic concept is that we regress the annual mean global average net downward radiative flux (R) at the top of atmosphere (TOA) against the annual mean ΔSWV averaged at TLS, NH LMS, or SH LMS. The equilibrium ΔSWV is where the linear fit intercepts at R=0. Then we simply subtract ΔSWV_{fast} from the equilibrium ΔSWV to estimate equilibrium ΔSWV_{slow}.

These regressions can be very noisy and yield highly uncertain parameters, particularly for perturbations with relatively small amounts of radiative forcing and warming. To account for this, we first fit the R and ΔSWV time series using an exponential function ($y(t) = b + a1 \cdot e^{-t/\tau 1} + a2 \cdot e^{-t/\tau 2}$), and then do the regression using the fitted time series. For fully coupled models, we constrain $\tau 1$ to be within the range of 4 ± 2 years and $\tau 2$ to be within the range of 250 ± 70 years; for CAM4, in which the atmosphere is coupled to a slab ocean, we constrain $\tau 1$ to be within the range of 4 ± 2 years. We then compute the best fit of all parameters. The ranges for the time constants are based on previous estimations of climate system time scales (Geoffroy et al., 2013). We estimate the ΔSWV-intercept at R=0 by regressing the fitted R and ΔSWV data over the last 30 years, since the relation between R and ΔSWV is not necessarily linear over the entire 100-year period. The slow and fast responses of other variables, such as global average surface temperatures and cold point temperatures are computed using the same method.

We tested this method in a climate model that nearly reaches the equilibrium climate state. We analysed runs of the fully coupled Max Planck Institute Earth System Model version 1.1 (MPI-ESM1.1) (Maher et al., 2019), which has a transient climate response and an effective climate sensitivity near the middle of the CMIP5 ensemble range (Adams and Dessler, 2019; Dessler, 2020). It includes a 2000-year preindustrial control run and a 2614-year abruptly quadrupled CO_2 run. The values of ΔSWV averaged over the last 30 years of the $4xCO_2$ run relative to the control run are 4.60 ppmv in the TLS, 22.40 ppmv in the NH LMS, and 9.69 ppmv in the SH LMS. We expect this to be close to equilibrium ΔSWV because the trend in global average surface temperature over the last 500 years of the $4xCO_2$ run is 0.02 K per century. We use the regression method to estimate the equilibrium ΔSWV using MPI-ESM1.1 water vapor mixing ratio time series over the first 100 years and obtain estimates of 4.38 ppmv in the TLS, 20.01 ppmv in the NH LMS, and 9.07 ppmv in the SH LMS; these yield

https://doi.org/10.5194/acp-2020-495
Preprint. Discussion started: 29 June 2020

differences of 0.22 ppmv in the TLS, 2.39 ppmv in the NH LMS, and 0.62 ppmv in the SH LMS. Thus, our method underestimates the true equilibrium value by 5% in the TLS, 11% in the NH LMS, and 6% in the SH LMS.

Uncertainty for slow and fast responses of different quantities shown in this paper are obtained from Monte Carlo samples as follows: For each perturbation, we randomly sample with replacement 100,000 times for each model that performed that perturbation and from these samples compute the 2.5%-97.5% percentiles.

3. Results

3.1 The slow stratospheric water vapor response

We show equilibrium ΔSWV_{slow} and its percentage contribution to the total equilibrium ΔSWV in Figure 1. We show results in the TLS (Figs. 1a and 1d), in the NH LMS (Figs. 1b and 1e), and the SH LM (Figs. 1c and 1f). In evaluating the absolute magnitude of ΔSWV_{slow} in the first column of Fig. 1, we normalize the equilibrium ΔSWV_{slow} using effective radiative forcing (ERF), so that differences in the magnitude of the forcing do not confound our results.

ERF values used in construction of Fig. 1 are plotted in Fig. 2a; they are calculated as the difference in net radiation at the top of atmosphere (TOA) after the atmospheric perturbation (e.g., the addition of CO_2), but before the surface has warmed. In all cases, we calculate this by differencing the average of the last 10 years of the fixed SST run with the perturbed atmosphere from the same quantity in the fixed SST run with the baseline atmosphere. The equilibrium global averaged surface temperature changes (ΔTs), estimated using the regression method described in Section 2.2 and normalized by ERF, are plotted in Fig. 2b. The ensemble average ΔTs/ERF shows general agreement across different perturbations. This quantity is the inverse of the feedback parameter λ (e.g. Dessler and Zelinka, 2015), so Fig. 2b implies that the climate sensitivity to these different perturbations is similar (Richardson et al., 2019). We also list the quantities for each model and perturbation in Table S1.

In each region, the magnitude of ensemble average ΔSWV_{slow}/ERF shows general agreement for different perturbations. The magnitudes of ΔSWV_{slow}/ERF in the LMS tend to be larger than those in the TLS (Figs. 1b-c). This is consistent with previous studies, which showed that the long-term trend in SWV over the century in climate models is largest near the LMS tropopause (Dessler et al., 2013; Huang et al., 2016; Banerjee et al., 2019). This reflects different transport pathways into the LMS, including the downward transport by the Brewer-Dobson circulation, quasi-horizontal isentropic mixing from tropical troposphere, and convective influence (Dessler et al., 1995; Holton et al., 1995; Plumb, 2002; Gettelman et al., 2011).

In the LMS, the ensemble average $\Delta SWV_{slow}/\Delta SWV$ ratio is close to 100% for many perturbations (Figs. 1e-f). In the TLS, the ensemble average $\Delta SWV_{slow}/\Delta SWV$ ratio is generally above 50%, with a few exceptions. We will discuss this in detail in

https://doi.org/10.5194/acp-2020-495
Preprint. Discussion started: 29 June 2020

Section 3.3.

We note that inter-model variability in ΔSWV_{slow}/ERF and ΔSWV_{slow} is generally consistent for different perturbations. For example, HadGEM3 produces larger responses than the rest of the ensemble for most perturbations (Figs. 1a-c, Table S1), likely connected to larger surface warming per ERF than the rest of the ensemble (Fig. 2b). GISS-E2-R and MIROC-SPRINTARS have ΔSWV_{slow}/ERF and ΔSWV_{slow} values generally below the rest of the ensemble (Figs. 1a-c, Table S1), likely connected to smaller surface temperature changes per ERF (Fig. 2b).

3.2 The slow stratospheric water vapor response and the surface temperature change

Our results show that, in most climate perturbations analyzed in this study, the equilibrium response of water vapor in both the TLS and the LMS is dominated by ΔSWV_{slow}, which is the component mediated by surface temperature change. To directly quantify how SWV responds to surface temperature across a range of different climate change mechanisms, we linearly regress the time series of annual mean ΔSWV_{slow} over the entire period of the coupled simulations (at least 100 years) against the time series of annual mean global averaged surface temperature change (ΔTs). This is similar to the analysis of Banerjee et al. (2019), who did this for quadrupled CO_2 perturbation, but we do this for multiple perturbations.

The scatter plot for each perturbation and model is shown in supplement (Figures S1-3). For most perturbations and models, the ΔSWV_{slow} time series in both the TLS and the LMS is positively correlated with the ΔTs time series, supporting the hypothesis that the surface temperature change contributes to the long-term trend in SWV for most cases.

Figure 3 shows the slopes of the regression for all perturbations and models. The ensemble average and uncertainty of the slopes are obtained from Monte Carlo samples: For each model and perturbation, we first randomly sample the slope 100,000 times, assuming a Gaussian distribution. Then, for each perturbation, we sample from the slope distributions with replacement 100,000 times for each model that performed that perturbation and from these samples compute the ensemble mean and 2.5%-97.5% percentiles.

In both the TLS and LMS, the slopes from different perturbations show general agreement (Fig. 3). In the TLS, the ensemble and perturbation average slope is 0.35 ppmv K^{-1} with a 95% confidence interval of 0.28-0.44 ppmv K^{-1} (Fig. 3a). The LMS ΔSWV_{slow} time series has stronger correlations with the ΔTs time series (Figures S1-3) and produces larger sensitivities (Figs. 3b-c). Specifically, the ensemble and perturbation average slope is 2.1 ppmv K^{-1} in the NH, and is 0.97 ppmv K^{-1} in the SH, with 95% confidence intervals of 1.82-2.39 ppmv K^{-1} and 0.79-1.15 ppmv K^{-1}, respectively. The larger LMS SWV sensitivity reflects a different mix of transport pathways into the LMS compared to the TLS (Dessler et al., 1995; Holton et al., 1995; Plumb, 2002; Gettelman et al., 2011). Our results are similar to those of Dessler et al. (2013) and Smalley et al. (2017) despite the fact that they used 500-hPa temperature as their regressor.

https://doi.org/10.5194/acp-2020-495
Preprint. Discussion started: 29 June 2020

Atmospheric Chemistry and Physics
Discussions

We show that the relation between ΔSWV_{slow} and ΔTs time series can be extended to the entire stratosphere (Figs. 4a). We re-gridded the zonal mean ΔSWV_{slow} from all models and perturbations onto the same pressure-latitude grid (10 hPa above 100 hPa and 50 hPa below 100 hPa, 4 degrees latitude) and regress the ΔSWV_{slow} time series at each grid point against global average ΔTs time series. The ensemble and perturbation average slope of the linear fit at each grid point is shown in Fig. 4a (Figures for each individual perturbation are shown in Fig. S4). Since the vertical gradient of water vapor is large, we plot the percentage change of mixing ratio per degree K relative to the baseline. Lapse rate tropopause, the lowest level where the lapse rate decreases to 2 K km^{-1}, also plotted, is obtained using the atmospheric temperatures from the baseline coupled run and ensemble averaged.

We clearly see the larger sensitivity of ΔSWV_{slow} to ΔTs in the LMS than in the overworld. In the LMS, the slope has a hemispheric asymmetry, with larger values in the NH. This is consistent with previous studies, which showed that isentropic transport brings more tropospheric water vapor to the NH than the SH (Pan et al., 1997, 2000; Dethof et al., 1999, 2000; Ploeger et al., 2013). In addition, convective moistening may be more important to the NH due to more land in the NH and, consequently, more convection (Dessler and Sherwood, 2004; Smith et al., 2017; Ueyama et al., 2018; Wang et al., 2019). We see large values in the tropical upper troposphere, which is the main part of the tropospheric water vapor feedback. The sensitivity declines as one ascends through the TTL. Once above the TTL, the sensitivity in the overworld is relatively uniform with altitude.

3.3 The fast stratospheric water vapor response

Figure 1 also shows the ΔSWV_{fast} normalized by the ERF (Figs. 1g-i) as well as its contribution to total equilibrium ΔSWV (Figs. 1j-l). As discussed previously, ΔSWV_{fast} is the change in SWV due to the perturbation, but before the surface temperature has responded. For most perturbations, especially in the LMS, $\Delta SWV_{fast}/ERF$ is smaller than $\Delta SWV_{slow}/ERF$, with a magnitude of a few tenths of a ppmv·(Wm^{-2})$^{-1}$.

For 2xCO_2, the near-zero TLS $\Delta SWVf_{ast}/ERF$ is the result of cancellation between cooling by a strengthening Brewer-Dobson circulation and increased local radiative heating (Lin et al., 2017). Some other GHG forcing agents, however, produce larger TLS $\Delta SWV_{fast}/ERF$ and contributions in the TLS. The ensemble average ΔSWV_{fast} from 10xCFC-12 and 10xCFC-11 contribute about half of the total ΔSWV, respectively (Fig. 1j). This is a consequence of halocarbons producing more TTL warming per Wm^{-2} by efficiently absorbing upwelling longwave radiation from the troposphere in the atmospheric window (Jain et al., 2000). Fig. 5 shows the fast temperature response per unit ERF due to different perturbations and it shows heating in the TTL for both 10xCFC-12 and 10xCFC-11.

Increases of tropospheric O_3 (5xO_3) reduce the shortwave radiation absorption by stratospheric O_3, which cools the stratosphere (Fig. 5). Meanwhile, the O_3 in the upper troposphere absorbs short wave radiation and heats the TTL (Fig. 5), which results in larger TLS ΔSWV_{fast}/ERF magnitude than ΔSWV_{slow}/ERF and larger contributions to total equilibrium ΔSWV (77%) (Figs. 1g and 1j). Tropospheric O_3 is also transported to the LMS region, which heats the LMS by absorbing short wave radiation and results in larger LMS ΔSWV_{fast}/ERF magnitude than ΔSWV_{slow}/ERF (Figs. 1h-j). We note that our conclusion on $5xO_3$ is based on only one model, MIROC-SPRINTARS.

The $3xCH_4$ also includes multiple models that produce larger TLS ΔSWV_{fast}/ERF magnitudes and contributions than ΔSWV_{slow}/ERF. Figure 5 shows TTL heating for $3xCH_4$. The TTL heating could be due to the shortwave absorption by CH_4, which is explicitly treated in models including CAM5, CanESM2, MPI-ESM, and MIROC-SPRINTARS (Smith et al., 2018). These models are also the ones that produce TLS ΔSWV_{fast} contributions larger than 50% in $3xCH_4$ (Figs. 1g and 1j).

ΔSWV_{fast} from 10xBC dominates total equilibrium ΔSWV in the TLS, with ensemble average contribution of 84%. The magnitude of the ensemble average ΔSWV_{fast}/ERF from 10xBC is also larger than any other perturbations in each region. This occurs because the 10xBC strongly absorbs shortwave radiation, causing large heating of the tropopause region in both the tropics and extra-tropics. Figure 5 shows the 10xBC gives by far the most warming per unit ERF.

The 10xBC ΔSWV_{fast}/ERF in the NH and SH LMS contributes to about 50% of the total equilibrium ΔSWV, with smaller magnitudes in the SH (Figs. 1h-i and 1k-l). This is because the total amount of black carbon is smaller in the SH (Myhre et al., 2017), since black carbon is a combustion product and is predominantly emitted over the NH continents (Ramanathan and Carmichael, 2008). The 10xBCSLT ΔSWV_{fast} also contributes about 50% of the total 10xBCSLT ΔSWV. The 10xBCSLT does not produce as strong a ΔSWV_{fast}/ERF as 10xBC, since the reduction in BC lifetime leads to less BC in the TTL and therefore less heating per unit ERF.

We quantify control of TLS ΔSWV_{fast} by the fast TTL temperature adjustments across a range of different climate perturbations by regressing the TLS ΔSWV_{fast} against the fast response of the cold point temperature (ΔTCP_{fast}). To estimate ΔTCP_{fast} in the models, we first find the minimum temperature in the profile at each grid point in the fixed SST runs (no interpolation is done, we simply find the minimum temperature on the output model levels). These minimum temperatures are then averaged between 30°N – 30°S to yield TCP_{fast} in each run. ΔTCP_{fast} is the difference between TCP_{fast} in the perturbed model run minus that in the baseline runs.

We find that TLS ΔSWV_{fast} is strongly correlated with ΔTCP_{fast} across all perturbations and models (Fig. 6a), with a slope of 0.52 ppmv K^{-1} and a 95% confidence interval of 0.43 to 0.61 ppmv K^{-1}. Randel and Park (2019) pointed out that the slope from the Clausius-Clapeyron relationship evaluated near the tropical tropopause is close to this value, about 0.5 ppmv K^{-1}.

We also separately plot the slopes between ΔSWV_{fast} and ΔTCP_{fast} for each perturbation (Figs. 6d-f). For the perturbations that have more than five participating models, including $2xCO_2$, $3xCH_4$, 2%Solar, 10xBC, $5xSO_4$, and 10xCFC-12, we

https://doi.org/10.5194/acp-2020-495
Preprint. Discussion started: 29 June 2020

calculate the linear regression between ΔSWV_{fast} and ΔTCP_{fast} from the models and show the slopes and 95% confidence intervals. For the perturbations that have fewer participating models, including 10xCFC11, $3xN_2O$, $5xO_3$, and 10xBCSLT, we plot the ratio $\Delta SWV_{fast}/\Delta TCP_{fast}$ and show only the ensemble averages. The slopes produced by different perturbations show general agreement (Fig. 6d). The larger uncertainty in the slopes produced by 2%Solar and 10xCFC-12 occurs because both the ΔTCP_{fast} and ΔSWV_{fast} produced by different models are similar and therefore the slope of the linear regression is uncertain. Overall, we find that the fast response of TTL temperature is a good predictor for the TLS ΔSWV_{fast} across a range of different climate mechanisms and across multiple models.

For the LMS ΔSWV_{fast}, the ΔTCP_{fast} does not show a control as strong as that in the TLS (Figs. 6b-c) due to the fact that TTL temperatures are only one factor that influences the LMS. In addition, the regression between ΔSWV_{fast} and ΔTCP_{fast} across all perturbations at each grid point in the pressure-latitude domain shows that the slope (% K^{-1}) follows the transport pattern of the BDC (Fig. 4b). The slope is large in the tropical overworld stratosphere and become weaker as one moves poleward and downward in the extra-tropics below 150 hPa. The value is lower in the LMS, again consistent with the fact that water vapor in the LMS is controlled by several processes, not just TTL cold-point temperature. Clearly, more work on this is warranted.

Summary

It is of great interest for the climate community to understand how SWV changes when the climate changes since SWV plays an important role in the Earth's radiative budget and stratospheric ozone chemistry (Solomon et al., 1986, 2010; Dvortsov and Solomon, 2001; Forster and Shine, 2002). In this study, we investigate the response of stratospheric water vapor (SWV) to a range of different climate forcing mechanisms using a multi-model and multiple forcing agent framework. We use output from nine CMIP5 models participating the PDRMIP. Each model performs a baseline and up to 10 climate perturbation experiments, including $2xCO_2$, $3xCH_4$, 2%Solar, 10xBC, $5xSO_4$, 10xCFC-11, 10xCFC-12, $3xN_2O$, $5xO_3$, and 10xBCSLT (Table 1). Each perturbation is performed in two configurations, including fixed SST simulations (at least 15 years) and fully coupled simulations (at least 100 years).

To better understand the SWV response (ΔSWV), we partition it into two parts: the slow response (ΔSWV_{slow}) and the fast response (ΔSWV_{fast}). The ΔSWV_{fast} is the change in response to a perturbation on short time scales, before the surface temperature has responded. ΔSWV_{slow} occurs on longer time scales and is coupled to the surface temperature change. Our results show that, for most perturbations, ΔSWV in the tropical lower stratosphere (TLS) and in the lowermost stratosphere (LMS) (200 hPa, 50°N-90°N and 50°S-90°S) is dominated by ΔSWV_{slow} (Fig. 1).

Analysis of ΔSWV_{slow} shows that a warming surface increases SWV (Figures S1-3). Furthermore, the response of SWV to the surface temperature change has a similar sensitivity across different climate perturbations in both the overworld

https://doi.org/10.5194/acp-2020-495
Preprint. Discussion started: 29 June 2020

stratosphere and the lowermost stratosphere (Figs. 3 and 4a). Specifically, the ensemble and perturbation average slope is 0.35 ppmv K^{-1} in the TLS, 2.1 ppmv K^{-1} in the northern hemispheric (NH) LMS, and 0.97 ppmv K^{-1} in the southern hemispheric (SH) LMS (Fig. 3).

ΔSWV_{slow} in the LMS is more sensitive to ΔTs than the tropical overworld, reflecting different transport pathways into the LMS compared to the overworld (Dessler et al., 1995; Holton et al., 1995; Plumb, 2002; Gettelman et al., 2011). The ΔSWV_{slow} in the NH LMS is even more sensitive, consistent with hemispheric asymmetries in the isentropic transport and convective moistening reported by previous studies (Pan et al., 1997, 2000; Dethof et al., 1999, 2000; Dessler and Sherwood, 2004; Ploeger et al., 2013; Smith et al., 2017; Ueyama et al., 2018; Wang et al., 2019).

The fast response of SWV from most perturbations are weak compared to the slow response and therefore plays a smaller role in ΔSWV (Fig. 1). However, for forcing agents that directly heat tropopause levels (Fig. 5), ΔSWV_{fast} makes a larger contribution to ΔSWV. In particular, when climate is perturbed by 10xBC, the ΔSWV_{fast} dominates the ΔSWV_{slow} and has larger magnitude than any other perturbed simulations in both the TLS and LMS. This occurs because black carbon absorbs shortwave radiation in the atmosphere and directly heats the temperatures at tropopause levels. Other forcing agents also heat the tropopause levels and increase ΔSWV_{fast} through absorption of shortwave radiation or longwave radiation at the atmospheric window range (3xCH_4, 5xO_3, 10xBCSLT, 10xCFC-12, 10xCFC-11), but are not as strong as 10xBC.

The TLS ΔSWV_{fast} is controlled by the fast response of the cold point temperature across different climate change mechanisms (Fig. 6), with a slope of 0.52 ppmv K^{-1}, which is consistent with the Clausius-Clapeyron relationship evaluated near the tropical tropopause (Randel and Park, 2019). The control of cold point temperature fast response over ΔSWV_{fast} is stronger in the tropical overworld and becomes weaker at higher latitudes in the LMS below 150 hPa (Fig. 4b).

Data availability: The PDRMIP data can be downloaded from this website: https://cicero.oslo.no/en/PDRMIP.

Competing interests. The authors declare that they have no conflict of interest.

Author contribution: Xun Wang performed analyses and wrote the original draft. Andrew E. Dessler provided the conceptualization, guidance, and editing.

Acknowledgments: This work was supported by NASA grants 80NSSC18K0134 and 80NSSC19K0757. This work was also supported by the National Center for Atmospheric Research, which is a major facility sponsored by the National Science Foundation under Cooperative Agreement No. 1852977. Any opinions, findings and conclusions or recommendations expressed in this material do not necessarily reflect the views of the National Science Foundation. We would like to acknowledge the PDRMIP modelling groups. We acknowledge helpful discussions with Andrew Gettelman and William Randel.

https://doi.org/10.5194/acp-2020-495
Preprint. Discussion started: 29 June 2020

References.

Adams, B. K. and Dessler, A. E.: Estimating Transient Climate Response in a Large-Ensemble Global Climate Model Simulation, Geophys. Res. Lett., 46(1), 311–317, doi:10.1029/2018GL080714, 2019.

Arora, V. K., Scinocca, J. F., Boer, G. J., Christian, J. R., Denman, K. L., Flato, G. M., Kharin, V. V., Lee, W. G. and Merryfield, W. J.: Carbon emission limits required to satisfy future representative concentration pathways of greenhouse gases, Geophys. Res. Lett., 38(5), n/a-n/a, doi:10.1029/2010GL046270, 2011.

Banerjee, A., Chiodo, G., Previdi, M., Ponater, M., Conley, A. J. and Polvani, L. M.: Stratospheric water vapor: an important climate feedback, Clim. Dyn., doi:10.1007/s00382-019-04721-4, 2019.

Bellouin, N., Rae, J., Jones, A., Johnson, C., Haywood, J. and Boucher, O.: Aerosol forcing in the Climate Model Intercomparison Project (CMIP5) simulations by HadGEM2-ES and the role of ammonium nitrate, J. Geophys. Res., 116(D20), D20206, doi:10.1029/2011JD016074, 2011.

Brasseur, G. P. and Solomon, S.: Aeronomy of the Middle Atmosphere, Springer Netherlands, Dordrecht., 2005.

Collins, W. J., Bellouin, N., Doutriaux-Boucher, M., Gedney, N., Halloran, P., Hinton, T., Hughes, J., Jones, C. D., Joshi, M., Liddicoat, S., Martin, G., O'Connor, F., Rae, J., Senior, C., Sitch, S., Totterdell, I., Wiltshire, A. and Woodward, S.: Development and evaluation of an Earth-System model – HadGEM2, Geosci. Model Dev., 4(4), 1051–1075, doi:10.5194/gmd-4-1051-2011, 2011.

Dessler, A. E.: Potential Problems Measuring Climate Sensitivity from the Historical Record, J. Clim., 33(6), 2237–2248, doi:10.1175/JCLI-D-19-0476.1, 2020.

Dessler, A. E. and Sherwood, S. C.: Effect of convection on the summertime extratropical lower stratosphere, J. Geophys. Res. Atmos., 109(D23), doi:10.1029/2004JD005209, 2004.

Dessler, A. E. and Zelinka, M. D.: Climate Feedbacks, in Encyclopedia of Atmospheric Sciences, edited by P. J. North G. R. and F. Zhang, Academic Press, Oxford., n.d.

Dessler, A. E., Hintsa, E. J., Weinstock, E. M., Anderson, J. G. and Chan, K. R.: Mechanisms controlling water vapor in the lower stratosphere: "A tale of two stratospheres," J. Geophys. Res., 100(D11), 23167, doi:10.1029/95JD02455, 1995.

Dessler, A. E., Schoeberl, M. R., Wang, T., Davis, S. M. and Rosenlof, K. H.: Stratospheric water vapor feedback, Proc. Natl. Acad. Sci., 110(45), 18087–18091, doi:10.1073/pnas.1310344110, 2013.

Dessler, A. E., Ye, H., Wang, T., Schoeberl, M. R., Oman, L. D., Douglass, A. R., Butler, A. H., Rosenlof, K. H., Davis, S. M. and Portmann, R. W.: Transport of ice into the stratosphere and the humidification of the stratosphere over the 21st century, Geophys. Res. Lett., 43(5), 2323–2329, doi:10.1002/2016GL067991, 2016.

Dethof, A., O'Neill, A., Slingo, J. M. and Smit, H. G. J.: A mechanism for moistening the lower stratosphere involving the Asian summer monsoon, Q. J. R. Meteorol. Soc., 125(556), 1079–1106, doi:10.1002/qj.1999.49712555602, 1999.

Dethof, A., O'Neill, A. and Slingo, J.: Quantification of the isentropic mass transport across the dynamical tropopause, J. Geophys. Res. Atmos., 105(D10), 12279–12293, doi:10.1029/2000JD900127, 2000.

Dufresne, J.-L., Foujols, M.-A., Denvil, S., Caubel, A., Marti, O., Aumont, O., Balkanski, Y., Bekki, S., Bellenger, H., Benshila, R., Bony, S., Bopp, L., Braconnot, P., Brockmann, P., Cadule, P., Cheruy, F., Codron, F., Cozic, A., Cugnet, D., de Noblet, N., Duvel, J.-P., Ethé, C., Fairhead, L., Fichefet, T., Flavoni, S., Friedlingstein, P., Grandpeix, J.-Y., Guez, L., Guilyardi, E., Hauglustaine, D., Hourdin, F., Idelkadi, A., Ghattas, J., Joussaume, S., Kageyama, M., Krinner, G., Labetoulle, S., Lahellec, A., Lefebvre, M.-P., Lefevre, F., Levy, C., Li, Z. X., Lloyd, J., Lott, F., Madec, G., Mancip, M., Marchand, M., Masson, S., Meurdesoif, Y., Mignot, J., Musat, I., Parouty, S., Polcher, J., Rio, C., Schulz, M., Swingedouw, D., Szopa, S., Talandier, C., Terray, P., Viovy, N. and Vuichard, N.: Climate change projections using the IPSL-CM5 Earth System Model: from CMIP3 to CMIP5, Clim. Dyn., 40(9–10), 2123–2165, doi:10.1007/s00382-012-1636-1, 2013.

Dvortsov, V. L. and Solomon, S.: Response of the stratospheric temperatures and ozone to past and future increases in stratospheric humidity, J. Geophys. Res. Atmos., 106(D7), 7505–7514, doi:10.1029/2000JD900637, 2001.

Forster, P. M. de F. and Shine, K. P.: Assessing the climate impact of trends in stratospheric water vapor, Geophys. Res. Lett., 29(6), 10-1-10–4, doi:10.1029/2001GL013909, 2002.

Fueglistaler, S., Dessler, A. E., Dunkerton, T. J., Folkins, I., Fu, Q. and Mote, P. W.: Tropical tropopause layer, Rev. Geophys., 47, 1–31, doi:10.1029/2008RG000267, 2009.

Gent, P. R., Danabasoglu, G., Donner, L. J., Holland, M. M., Hunke, E. C., Jayne, S. R., Lawrence, D. M., Neale, R. B.,

Rasch, P. J., Vertenstein, M., Worley, P. H., Yang, Z.-L. and Zhang, M.: The Community Climate System Model Version 4, J. Clim., 24(19), 4973–4991, doi:10.1175/2011JCLI4083.1, 2011.
Geoffroy, O., Saint-Martin, D., Olivié, D. J. L., Voldoire, A., Bellon, G. and Tytéca, S.: Transient Climate Response in a Two-Layer Energy-Balance Model. Part I: Analytical Solution and Parameter Calibration Using CMIP5 AOGCM Experiments, J. Clim., 26(6), 1841–1857, doi:10.1175/JCLI-D-12-00195.1, 2013.
Gettelman, A., Hegglin, M. I., Son, S.-W., Kim, J., Fujiwara, M., Birner, T., Kremser, S., Rex, M., Añel, J. A., Akiyoshi, H., Austin, J., Bekki, S., Braesike, P., Brühl, C., Butchart, N., Chipperfield, M., Dameris, M., Dhomse, S., Garny, H., Hardiman, S. C., Jöckel, P., Kinnison, D. E., Lamarque, J. F., Mancini, E., Marchand, M., Michou, M., Morgenstern, O., Pawson, S., Pitari, G., Plummer, D., Pyle, J. A., Rozanov, E., Scinocca, J., Shepherd, T. G., Shibata, K., Smale, D., Teyssèdre, H. and Tian, W.: Multimodel assessment of the upper troposphere and lower stratosphere: Tropics and global trends, J. Geophys. Res., 115, D00M08, doi:10.1029/2009JD013638, 2010.
Gettelman, A., Hoor, P., Pan, L. L., Randel, W. J., Hegglin, M. I. and Birner, T.: THE EXTRATROPICAL UPPER TROPOSPHERE AND LOWER STRATOSPHERE, Rev. Geophys., 49(3), RG3003, doi:10.1029/2011RG000355, 2011.
Giorgetta, M. A., Jungclaus, J., Reick, C. H., Legutke, S., Bader, J., Böttinger, M., Brovkin, V., Crueger, T., Esch, M., Fieg, K., Glushak, K., Gayler, V., Haak, H., Hollweg, H.-D., Ilyina, T., Kinne, S., Kornblueh, L., Matei, D., Mauritsen, T., Mikolajewicz, U., Mueller, W., Notz, D., Pithan, F., Raddatz, T., Rast, S., Redler, R., Roeckner, E., Schmidt, H., Schnur, R., Segschneider, J., Six, K. D., Stockhause, M., Timmreck, C., Wegner, J., Widmann, H., Wieners, K.-H., Claussen, M., Marotzke, J. and Stevens, B.: Climate and carbon cycle changes from 1850 to 2100 in MPI-ESM simulations for the Coupled Model Intercomparison Project phase 5, J. Adv. Model. Earth Syst., 5(3), 572–597, doi:10.1002/jame.20038, 2013.
Gregory, J. M.: A new method for diagnosing radiative forcing and climate sensitivity, Geophys. Res. Lett., 31(3), L03205, doi:10.1029/2003GL018747, 2004.
Holton, J. R., Haynes, P. H., McIntyre, M. E., Douglass, A. R., Rood, R. B. and Pfister, L.: Stratosphere-troposphere exchange, Rev. Geophys., 33(4), 403, doi:10.1029/95RG02097, 1995.
Hoskins, B. J.: Towards a PV-θ view of the general circulation, Tellus A Dyn. Meteorol. Oceanogr., 43(4), 27–36, doi:10.3402/tellusa.v43i4.11936, 1991.
Huang, Y., Zhang, M., Xia, Y., Hu, Y. and Son, S.-W.: Is there a stratospheric radiative feedback in global warming simulations?, Clim. Dyn., 46(1–2), 177–186, doi:10.1007/s00382-015-2577-2, 2016.
Hurrell, J. W., Holland, M. M., Gent, P. R., Ghan, S., Kay, J. E., Kushner, P. J., Lamarque, J.-F., Large, W. G., Lawrence, D., Lindsay, K., Lipscomb, W. H., Long, M. C., Mahowald, N., Marsh, D. R., Neale, R. B., Rasch, P., Vavrus, S., Vertenstein, M., Bader, D., Collins, W. D., Hack, J. J., Kiehl, J. and Marshall, S.: The Community Earth System Model: A Framework for Collaborative Research, Bull. Am. Meteorol. Soc., 94(9), 1339–1360, doi:10.1175/BAMS-D-12-00121.1, 2013.
Jain, A. K., Briegleb, B. P., Minschwaner, K. and Wuebbles, D. J.: Radiative forcings and global warming potentials of 39 greenhouse gases, J. Geophys. Res. Atmos., 105(D16), 20773–20790, doi:10.1029/2000JD900241, 2000.
Kay, J. E., Deser, C., Phillips, A., Mai, A., Hannay, C., Strand, G., Arblaster, J. M., Bates, S. C., Danabasoglu, G., Edwards, J., Holland, M., Kushner, P., Lamarque, J.-F., Lawrence, D., Lindsay, K., Middleton, A., Munoz, E., Neale, R., Oleson, K., Polvani, L. and Vertenstein, M.: The Community Earth System Model (CESM) Large Ensemble Project: A Community Resource for Studying Climate Change in the Presence of Internal Climate Variability, Bull. Am. Meteorol. Soc., 96(8), 1333–1349, doi:10.1175/BAMS-D-13-00255.1, 2015.
Lin, P., Paynter, D., Ming, Y. and Ramaswamy, V.: Changes of the Tropical Tropopause Layer under Global Warming, J. Clim., 30(4), 1245–1258, doi:10.1175/JCLI-D-16-0457.1, 2017.
MacIntosh, C. R., Allan, R. P., Baker, L. H., Bellouin, N., Collins, W., Mousavi, Z. and Shine, K. P.: Contrasting fast precipitation responses to tropospheric and stratospheric ozone forcing, Geophys. Res. Lett., 43(3), 1263–1271, doi:10.1002/2015GL067231, 2016.
Maher, N., Milinski, S., Suarez-Gutierrez, L., Botzet, M., Dobrynin, M., Kornblueh, L., Kröger, J., Takano, Y., Ghosh, R., Hedemann, C., Li, C., Li, H., Manzini, E., Notz, D., Putrasahan, D., Boysen, L., Claussen, M., Ilyina, T., Olonscheck, D., Raddatz, T., Stevens, B. and Marotzke, J.: The Max Planck Institute Grand Ensemble: Enabling the Exploration of Climate System Variability, J. Adv. Model. Earth Syst., 11(7), 2050–2069, doi:10.1029/2019MS001639, 2019.

https://doi.org/10.5194/acp-2020-495
Preprint. Discussion started: 29 June 2020

Martin, T. H. D. T. G. M., Bellouin, N., Collins, W. J., Culverwell, I. D., Halloran, P. R., Hardiman, S. C., Hinton, T. J., Jones, C. D., McDonald, R. E., McLaren, A. J., O'Connor, F. M., Roberts, M. J., Rodriguez, J. M., Woodward, S., Best, M. J., Brooks, M. E., Brown, A. R., Butchart, N., Dearden, C., Derbyshire, S. H., Dharssi, I., Doutriaux-Boucher, M., Edwards, J. M., Falloon, P. D., Gedney, N., Gray, L. J., Hewitt, H. T., Hobson, M., Huddleston, M. R., Hughes, J., Ineson, S., Ingram, W. J., James, P. M., Johns, T. C., Johnson, C. E., Jones, A., Jones, C. P., Joshi, M. M., Keen, A. B., Liddicoat, S., Lock, A. P., Maidens, A. V, Manners, J. C., Milton, S. F., Rae, J. G. L., Ridley, J. K., Sellar, A., Senior, C. A., Totterdell, I. J., Verhoef, A., Vidale, P. L. and Wiltshire, A.: The HadGEM2 family of Met Office Unified Model climate configurations, Geosci. Model Dev., 4(3), 723–757, doi:10.5194/gmd-4-723-2011, 2011.

Mote, P. W., Rosenlof, K. H., McIntyre, M. E., Carr, E. S., Gille, J. C., Holton, J. R., Kinnersley, J. S., Pumphrey, H. C., Russell III, J. M. and Waters, J. W.: An atmospheric tape recorder: The imprint of tropical tropopause temperatures on stratospheric water vapor, J. Geophys. Res., 101(D2), 3989–4006, doi:10.1029/95JD03422, 1996.

Myhre, G., Samset, B. H., Schulz, M., Balkanski, Y., Bauer, S., Berntsen, T. K., Bian, H., Bellouin, N., Chin, M., Diehl, T., Easter, R. C., Feichter, J., Ghan, S. J., Hauglustaine, D., Iversen, T., Kinne, S., Kirkevåg, A., Lamarque, J.-F., Lin, G., Liu, X., Lund, M. T., Luo, G., Ma, X., van Noije, T., Penner, J. E., Rasch, P. J., Ruiz, A., Seland, Ø., Skeie, R. B., Stier, P., Takemura, T., Tsigaridis, K., Wang, P., Wang, Z., Xu, L., Yu, H., Yu, F., Yoon, J.-H., Zhang, K., Zhang, H. and Zhou, C.: Radiative forcing of the direct aerosol effect from AeroCom Phase II simulations, Atmos. Chem. Phys., 13(4), 1853–1877, doi:10.5194/acp-13-1853-2013, 2013.

Myhre, G., Forster, P. M., Samset, B. H., Hodnebrog, Ø., Sillmann, J., Aalbergsjø, S. G., Andrews, T., Boucher, O., Faluvegi, G., Fläschner, D., Iversen, T., Kasoar, M., Kharin, V., Kirkevåg, A., Lamarque, J.-F., Olivié, D., Richardson, T. B., Shindell, D., Shine, K. P., Stjern, C. W., Takemura, T., Voulgarakis, A. and Zwiers, F.: PDRMIP: A Precipitation Driver and Response Model Intercomparison Project—Protocol and Preliminary Results, Bull. Am. Meteorol. Soc., 98(6), 1185–1198, doi:10.1175/BAMS-D-16-0019.1, 2017.

Neale, R. B., Richter, J. H., Conley, A. J., Park, S., Lauritzen, P. H., Gettelman, A., Williamson, D. L., Rasch, P. J., Vavrus, S. J., Taylor, M. A., Collins, W. D., Zhang, M., and Lin, S.:Description of the NCAR Community Atmosphere Model (CAM 4.0), NCAR Technical Note, NCAR/TN-485+STR, Climate And Global Dynamics Division National Center For Atmospheric Research Boulder, Colorado, USA, 224 pp., 2010. Available at http://www.cesm.ucar.edu/models/ccsm4.0/cam/docs/description/cam4_desc.pdf

Otto-Bliesner, B. L., Brady, E. C., Fasullo, J., Jahn, A., Landrum, L., Stevenson, S., Rosenbloom, N., Mai, A. and Strand, G.: Climate Variability and Change since 850 CE: An Ensemble Approach with the Community Earth System Model, Bull. Am. Meteorol. Soc., 97(5), 735–754, doi:10.1175/BAMS-D-14-00233.1, 2016.

Pan, L., Solomon, S., Randel, W., Lamarque, J.-F., Hess, P., Gille, J., Chiou, E.-W. and McCormick, M. P.: Hemispheric asymmetries and seasonal variations of the lowermost stratospheric water vapor and ozone derived from SAGE II data, J. Geophys. Res. Atmos., 102(D23), 28177–28184, doi:10.1029/97JD02778, 1997.

Pan, L. L., Hintsa, E. J., Stone, E. M., Weinstock, E. M. and Randel, W. J.: The seasonal cycle of water vapor and saturation vapor mixing ratio in the extratropical lowermost stratosphere, J. Geophys. Res. Atmos., 105(D21), 26519–26530, doi:10.1029/2000JD900401, 2000.

Ploeger, F., Günther, G., Konopka, P., Fueglistaler, S., Müller, R., Hoppe, C., Kunz, A., Spang, R., Grooß, J.-U. and Riese, M.: Horizontal water vapor transport in the lower stratosphere from subtropics to high latitudes during boreal summer, J. Geophys. Res. Atmos., 118(14), 8111–8127, doi:10.1002/jgrd.50636, 2013.

Plumb, R. A.: Stratospheric Transport, J. Meteorol. Soc. Japan. Ser. II, 80(4B), 793–809, doi:10.2151/jmsj.80.793, 2002.

Ramanathan, V. and Carmichael, G.: Global and regional climate changes due to black carbon, Nat. Geosci., 1(4), 221–227, doi:10.1038/ngeo156, 2008.

Randel, W. and Park, M.: Diagnosing Observed Stratospheric Water Vapor Relationships to the Cold Point Tropical Tropopause, J. Geophys. Res. Atmos., 2019JD030648, doi:10.1029/2019JD030648, 2019.

Revell, L. E., Stenke, A., Rozanov, E., Ball, W., Lossow, S. and Peter, T.: The role of methane in projections of 21st century stratospheric water vapour, Atmos. Chem. Phys., 16(20), 13067–13080, doi:10.5194/acp-16-13067-2016, 2016.

Richardson, T. B., Forster, P. M., Smith, C. J., Maycock, A. C., Wood, T., Andrews, T., Boucher, O., Faluvegi, G., Fläschner, D., Hodnebrog, Ø., Kasoar, M., Kirkevåg, A., Lamarque, J. -F., Mülmenstädt, J., Myhre, G., Olivié, D., Portmann, R. W., Samset, B. H., Shawki, D., Shindell, D., Stier, P., Takemura, T., Voulgarakis, A. and Watson-Parris, D.: Efficacy of Climate Forcings in PDRMIP Models, J. Geophys. Res. Atmos., 124(23), 12824–12844,

doi:10.1029/2019JD030581, 2019.
Samset, B. H., Myhre, G., Forster, P. M., Hodnebrog, Ø., Andrews, T., Faluvegi, G., Fläschner, D., Kasoar, M., Kharin, V., Kirkevåg, A., Lamarque, J. -F., Olivié, D., Richardson, T., Shindell, D., Shine, K. P., Takemura, T. and Voulgarakis, A.: Fast and slow precipitation responses to individual climate forcers: A PDRMIP multimodel study, Geophys. Res. Lett., 43(6), 2782–2791, doi:10.1002/2016GL068064, 2016.
Schmidt, G. A., Kelley, M., Nazarenko, L., Ruedy, R., Russell, G. L., Aleinov, I., Bauer, M., Bauer, S. E., Bhat, M. K., Bleck, R., Canuto, V., Chen, Y.-H., Cheng, Y., Clune, T. L., Del Genio, A., de Fainchtein, R., Faluvegi, G., Hansen, J. E., Healy, R. J., Kiang, N. Y., Koch, D., Lacis, A. A., LeGrande, A. N., Lerner, J., Lo, K. K., Matthews, E. E., Menon, S., Miller, R. L., Oinas, V., Oloso, A. O., Perlwitz, J. P., Puma, M. J., Putman, W. M., Rind, D., Romanou, A., Sato, M., Shindell, D. T., Sun, S., Syed, R. A., Tausnev, N., Tsigaridis, K., Unger, N., Voulgarakis, A., Yao, M.-S. and Zhang, J.: Configuration and assessment of the GISS ModelE2 contributions to the CMIP5 archive, J. Adv. Model. Earth Syst., 6(1), 141–184, doi:10.1002/2013MS000265, 2014.
Sherwood, S. C., Bony, S., Boucher, O., Bretherton, C., Forster, P. M., Gregory, J. M. and Stevens, B.: Adjustments in the Forcing-Feedback Framework for Understanding Climate Change, Bull. Am. Meteorol. Soc., 96(2), 217–228, doi:10.1175/BAMS-D-13-00167.1, 2015.
Shu, J., Tian, W., Austin, J., Chipperfield, M. P., Xie, F. and Wang, W.: Effects of sea surface temperature and greenhouse gas changes on the transport between the stratosphere and troposphere, J. Geophys. Res., 116(D2), D02124, doi:10.1029/2010JD014520, 2011.
Smalley, K. M., Dessler, A. E., Bekki, S., Deushi, M., Marchand, M., Morgenstern, O., Plummer, D. A., Shibata, K., Yamashita, Y. and Zeng, G.: Contribution of different processes to changes in tropical lower-stratospheric water vapor in chemistry–climate models, Atmos. Chem. Phys., 17(13), 8031–8044, doi:10.5194/acp-17-8031-2017, 2017.
Smith, C. J., Kramer, R. J., Myhre, G., Forster, P. M., Soden, B. J., Andrews, T., Boucher, O., Faluvegi, G., Fläschner, D., Hodnebrog, Ø., Kasoar, M., Kharin, V., Kirkevåg, A., Lamarque, J. -F., Mülmenstädt, J., Olivié, D., Richardson, T., Samset, B. H., Shindell, D., Stier, P., Takemura, T., Voulgarakis, A. and Watson-Parris, D.: Understanding Rapid Adjustments to Diverse Forcing Agents, Geophys. Res. Lett., 45(21), doi:10.1029/2018GL079826, 2018.
Smith, J. B., Wilmouth, D. M., Bedka, K. M., Bowman, K. P., Homeyer, C. R., Dykema, J. A., Sargent, M. R., Clapp, C. E., Leroy, S. S., Sayres, D. S., Dean-Day, J. M., Paul Bui, T. and Anderson, J. G.: A case study of convectively sourced water vapor observed in the overworld stratosphere over the United States, J. Geophys. Res. Atmos., 122(17), 9529–9554, doi:10.1002/2017JD026831, 2017.
Solomon, S., Garcia, R. R., Rowland, F. S. and Wuebbles, D. J.: On the depletion of Antarctic ozone, Nature, 321(6072), 755–758, doi:doi:10.1038/321755a0, 1986.
Solomon, S., Rosenlof, K. H., Portmann, R. W., Daniel, J. S., Davis, S. M., Sanford, T. J. and Plattner, G.-K.: Contributions of Stratospheric Water Vapor to Decadal Changes in the Rate of Global Warming, Science (80-.)., 327(5970), 1219–1223, doi:10.1126/science.1182488, 2010.
Takemura, T., Nozawa, T., Emori, S., Nakajima, T. Y., Nakajima, T.: Simulation of climate response to aerosol direct and indirect effects with aerosol transport-radiation model, J. Geophys. Res., 110(D2), D02202, doi:10.1029/2004JD005029, 2005.
Takemura, T., Egashira, M., Matsuzawa, K., Ichijo, H., O'ishi, R. and Abe-Ouchi, A.: A simulation of the global distribution and radiative forcing of soil dust aerosols at the Last Glacial Maximum, Atmos. Chem. Phys., 9(9), 3061–3073, doi:10.5194/acp-9-3061-2009, 2009.
Tang, T., Shindell, D., Samset, B. H., Boucher, O., Forster, P. M., Hodnebrog, Ø., Myhre, G., Sillmann, J., Voulgarakis, A., Andrews, T., Faluvegi, G., Fläschner, D., Iversen, T., Kasoar, M., Kharin, V., Kirkevåg, A., Lamarque, J.-F., Olivié, D., Richardson, T., Stjern, C. W. and Takemura, T.: Dynamical response of Mediterranean precipitation to greenhouse gases and aerosols, Atmos. Chem. Phys., 18(11), 8439–8452, doi:10.5194/acp-18-8439-2018, 2018.
Tang, T., Shindell, D., Faluvegi, G., Myhre, G., Olivié, D., Voulgarakis, A., Kasoar, M., Andrews, T., Boucher, O., Forster, P. M., Hodnebrog, Ø., Iversen, T., Kirkevåg, A., Lamarque, J. -F., Richardson, T., Samset, B. H., Stjern, C. W., Takemura, T. and Smith, C.: Comparison of Effective Radiative Forcing Calculations Using Multiple Methods, Drivers, and Models, J. Geophys. Res. Atmos., 124(8), 4382–4394, doi:10.1029/2018JD030188, 2019.
Thuburn, J. and Craig, G. C.: On the temperature structure of the tropical substratosphere, J. Geophys. Res., 107(D2), 4017, doi:10.1029/2001JD000448, 2002.

https://doi.org/10.5194/acp-2020-495
Preprint. Discussion started: 29 June 2020

Atmospheric Chemistry and Physics Discussions

Ueyama, R., Jensen, E. J. and Pfister, L.: Convective Influence on the Humidity and Clouds in the Tropical Tropopause Layer During Boreal Summer, J. Geophys. Res. Atmos., doi:10.1029/2018JD028674, 2018.

Walters, D. N., Williams, K. D., Boutle, I. A., Bushell, A. C., Edwards, J. M., Field, P. R., Lock, A. P., Morcrette, C. J., Stratton, R. A., Wilkinson, J. M., Willett, M. R., Bellouin, N., Bodas-Salcedo, A., Brooks, M. E., Copsey, D., Earnshaw, P. D., Hardiman, S. C., Harris, C. M., Levine, R. C., MacLachlan, C., Manners, J. C., Martin, G. M., Milton, S. F., Palmer, M. D., Roberts, M. J., Rodríguez, J. M., Tennant, W. J. and Vidale, P. L.: The Met Office Unified Model Global Atmosphere 4.0 and JULES Global Land 4.0 configurations, Geosci. Model Dev., 7(1), 361–386, doi:10.5194/gmd-7-361-2014, 2014.

Wang, X., Dessler, A. E., Schoeberl, M. R., Yu, W. and Wang, T.: Impact of convectively lofted ice on the seasonal cycle of water vapor in the tropical tropopause layer, Atmos. Chem. Phys., 19(23), 14621–14636, doi:10.5194/acp-19-14621-2019, 2019.

Watanabe, M., Suzuki, T., O'ishi, R., Komuro, Y., Watanabe, S., Emori, S., Takemura, T., Chikira, M., Ogura, T., Sekiguchi, M., Takata, K., Yamazaki, D., Yokohata, T., Nozawa, T., Hasumi, H., Tatebe, H. and Kimoto, M.: Improved Climate Simulation by MIROC5: Mean States, Variability, and Climate Sensitivity, J. Clim., 23(23), 6312–6335, doi:10.1175/2010JCLI3679.1, 2010.

Xia, Y., Huang, Y., Hu, Y. and Yang, J.: Impacts of tropical tropopause warming on the stratospheric water vapor, Clim. Dyn., 53(5–6), 3409–3418, doi:10.1007/s00382-019-04714-3, 2019.

https://doi.org/10.5194/acp-2020-495
Preprint. Discussion started: 29 June 2020

Table 1: Description of PDRMIP models (Myhre et al., 2017) and list of perturbation experiments used in this study.

Model	Version	Resolution	Ocean setup	Aerosol setup	Key references	Perturbation experiments
Second Generation Canadian Earth System Model (CanESM2)	2010	2.8°×2.8°, 35 levels	Coupled ocean	Emissions	(Arora et al., 2011)	$2xCO_2$, $3xCH_4$, 2%Solar, 10xBC, $5xSO_4$
Community Earth System Model, version 1 (Community Atmosphere Model, version 4) [CESM1(CAM4)]	1.0.3	2.5°×1.9°, 26 levels	Slab ocean	Fixed concentrations	(Neale et al., 2010; Gent et al., 2011)	$2xCO_2$, $3xCH_4$, 2%Solar, 10xBC, $5xSO_4$, 10xCFC-12, $3xN_2O$, 10xBCSLT
CESM1 CAM5	1.1.2	2.5°×1.9°, 30 levels	Coupled ocean	Emissions	(Hurrell et al., 2013; Kay et al., 2015; Otto-Bliesner et al., 2016)	$2xCO_2$, $3xCH_4$, 2%Solar, 10xBC, $5xSO_4$, 10xCFC-12
Goddard Institute for Space Studies Model E2, coupled with the Russell ocean model (GISS-E2-R)	E2-R	2°×2.5°, 40 levels	Coupled ocean	Fixed concentrations	(Schmidt et al., 2014)	$2xCO_2$, $3xCH_4$, 2%Solar, 10xBC, $5xSO_4$, 10xCFC-12, 10xBCSLT
Hadley Centre Global Environment Model, version 2—Earth System (includes Carbon Cycle configuration with chemistry) (HadGEM2-ES)	6.6.3	1.875°×1.25°, 38 levels	Coupled ocean	Emissions	(Collins et al., 2011; Martin et al., 2011)	$2xCO_2$, $3xCH_4$, 2%Solar, 10xBC, $5xSO_4$, 10xCFC-12, 10xCFC-11, $3xN_2O$

https://doi.org/10.5194/acp-2020-495
Preprint. Discussion started: 29 June 2020

HadGEM3	Global Atmosphere 4.0	1.875°×1.25°, 85 levels	Coupled ocean	Fixed concentrations	(Bellouin et al., 2011; Walters et al., 2014)	$2xCO_2$, $3xCH_4$, 2%Solar, 10xBC, $5xSO_4$, 10xCFC-12
L'Institut Pierre-Simon Laplace Coupled Model, version 5A (IPSL-CM5A)	CMIP5	3.75° ×1.875°, 39 levels	Coupled ocean	Fixed concentrations	(Dufresne et al., 2013)	$2xCO_2$, $3xCH_4$, 2%Solar, 10xBC, $5xSO_4$
Max Planck Institute Earth System Model (MPI-ESM)	1.1.00p2	T63, 47 levels	Coupled ocean	Climatology, year 2000	(Giorgetta et al., 2013)	$2xCO_2$, $3xCH_4$, 2%Solar
Model for Interdisciplinary Research on Climate-Spectral Radiation-Transport Model for Aerosol Species (MIROC-SPRINTARS)	5.9.0	T85 (approx. 1.4°×1.4°), 40 levels	Coupled ocean	Hemispheric Transport Air Pollution, phase 2 Emissions	(Takemura, 2005; Takemura et al., 2009; Watanabe et al., 2010)	$2xCO_2$, $3xCH_4$, 2%Solar, 10xBC, $5xSO_4$, 10xCFC-12, 10xCFC-11, $3xN_2O$, $5xO_3$

https://doi.org/10.5194/acp-2020-495
Preprint. Discussion started: 29 June 2020

Atmospheric Chemistry and Physics
Open Access
Discussions

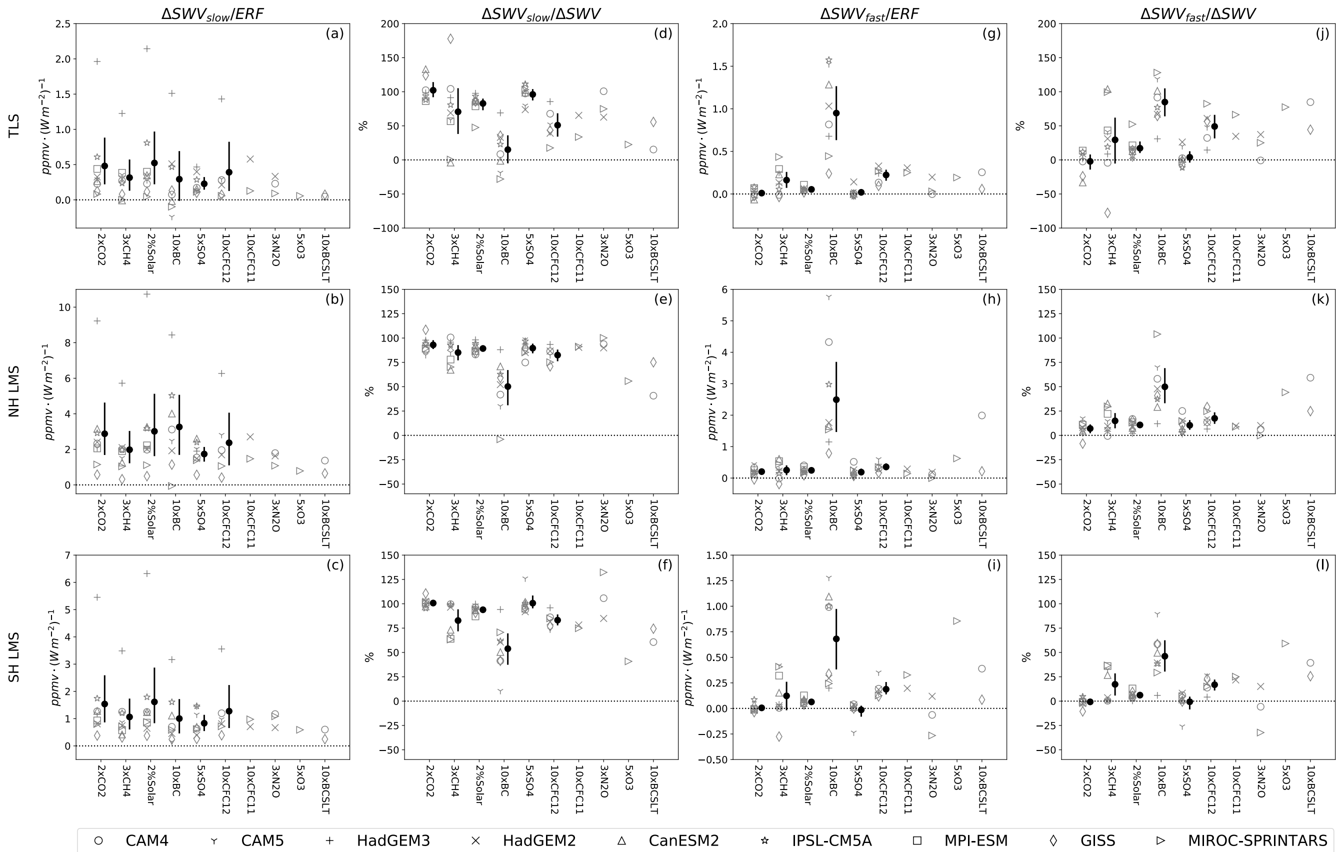

Figure 1. Panels (a)-(c): equilibrium ΔSWV_{slow} normalized by ERF ($ppmv \cdot (Wm^{-2})^{-1}$) in TLS (70 hPa, 30°N-30°S), NH LMS (200 hPa, 50°N-90°N), and SH LMS (200 hPa, 50°S-90°S). Panels (d)-(f): Contribution (%) of equilibrium ΔSWV_{slow} to total equilibrium ΔSWV. Panels (g)-(i): ΔSWV_{fast} normalized by ERF ($ppmv \cdot (Wm^{-2})^{-1}$). Panels (j)-(l): Contribution (%) of ΔSWV_{fast} to total equilibrium ΔSWV. The marker shapes indicate results from different models. The solid circles and error bars for each perturbation plotted in weighted black are ensemble average and 2.5%-97.5% confidence interval. Note that in the second and fourth columns, we took out models with extremely small ΔSWV magnitudes that yield extremely large $\Delta SWV_{slow}/\Delta SWV$ and $\Delta SWV_{fast}/\Delta SWV$ ratios.

https://doi.org/10.5194/acp-2020-495
Preprint. Discussion started: 29 June 2020

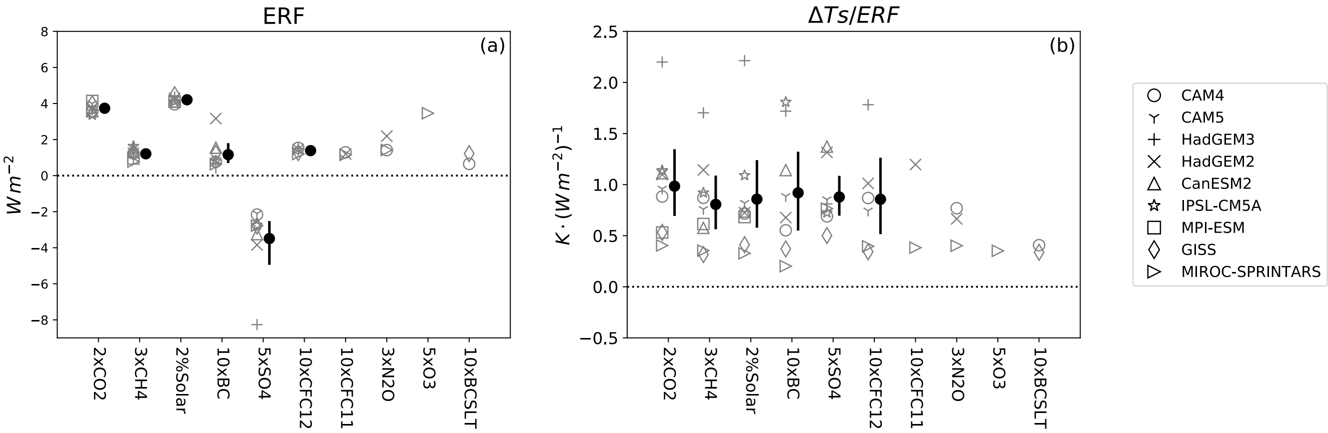

525 **Figure 2. Panel (a): Global average ERF (W m^{-2}) at the top of atmosphere. Panel (b): Global averaged surface temperature change per unit ERF (K·(W m^{-2})$^{-1}$). The marker shapes indicate results from different models. The solid circles and error bars for each perturbation plotted in weighted black are ensemble average and 2.5%-97.5% confidence intervals.**

https://doi.org/10.5194/acp-2020-495
Preprint. Discussion started: 29 June 2020

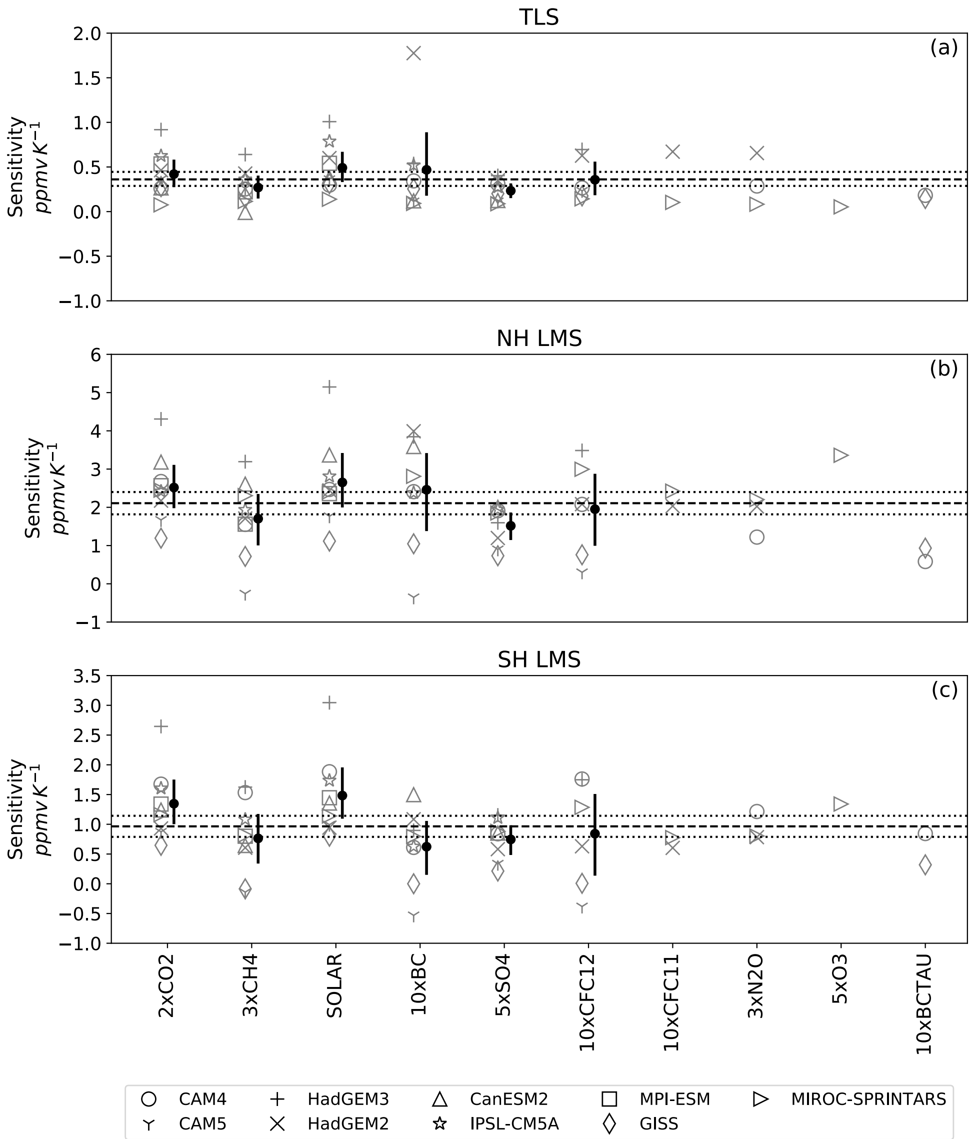

530 **Figure 3. Slopes (ppmv K^{-1}) from the linear regression between annual mean ΔSWV_{slow} time series and annual mean ΔTs time series. The marker shapes indicate results from different models. The solid circles and error bars for each perturbation plotted in weighted black are ensemble average and 2.5%-97.5% confidence intervals. The horizontal dashed line is the ensemble average of all slopes, and the horizontal dotted lines are 2.5%-97.5% confidence intervals.**

https://doi.org/10.5194/acp-2020-495
Preprint. Discussion started: 29 June 2020

Atmospheric Chemistry and Physics Discussions

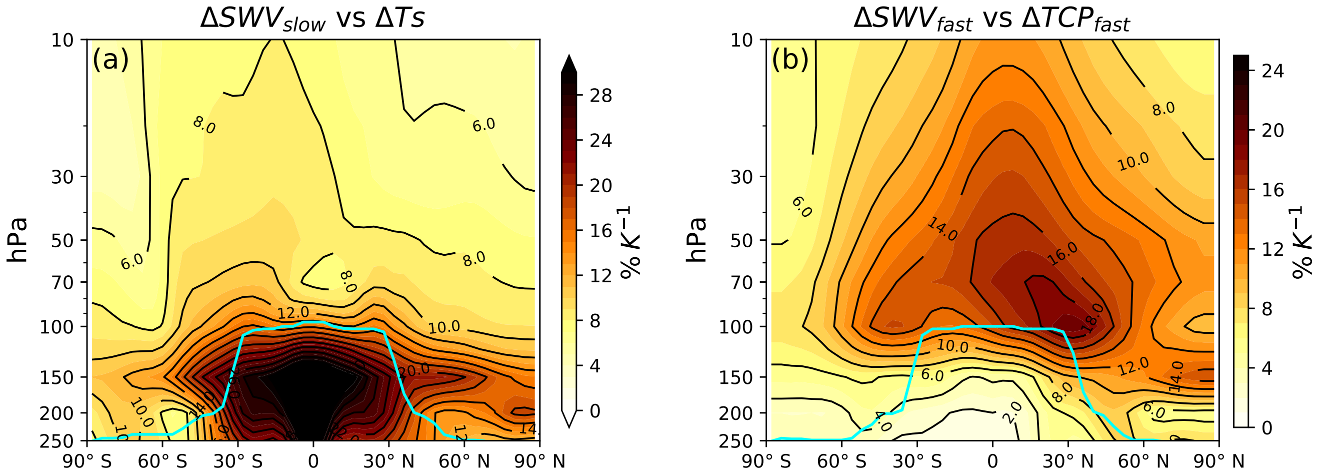

Figure 4. Panel (a): Ensemble and perturbation average slope (% K^{-1}) from the regression between annual mean time series of ΔSWV_{slow} at each latitude grid point and pressure level and annual mean time series of global average ΔTs. Panel (b): Slope (% K^{-1}) from the regression between ΔSWV_{fast} (ppmv) at each latitude grid point and pressure level and ΔTCP_{fast} (K). The solid cyan line is the ensemble average lapse rate tropopause derived from the baseline simulations.

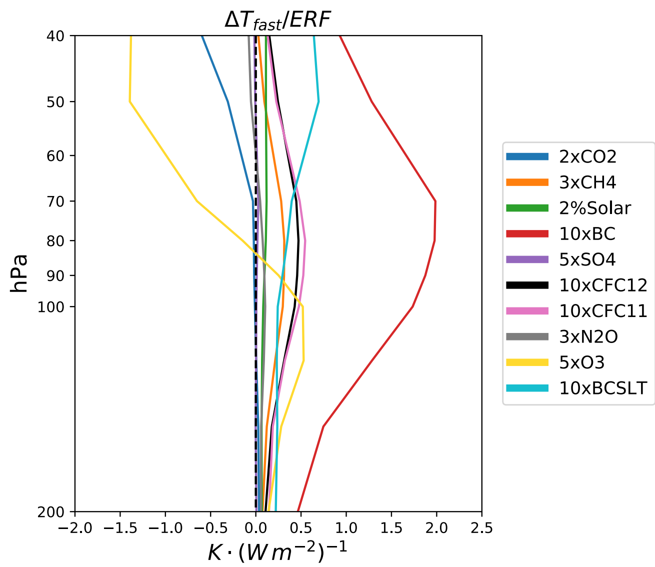

Figure 5. Profiles of fast temperature response normalized by ERF (K·(Wm^{-2})$^{-1}$) between 200 and 40 hPa, and averaged over 30°N-30°S. The color coding indicates results from different perturbations. Each profile is the ensemble average.

https://doi.org/10.5194/acp-2020-495
Preprint. Discussion started: 29 June 2020

Atmospheric Chemistry and Physics
Discussions

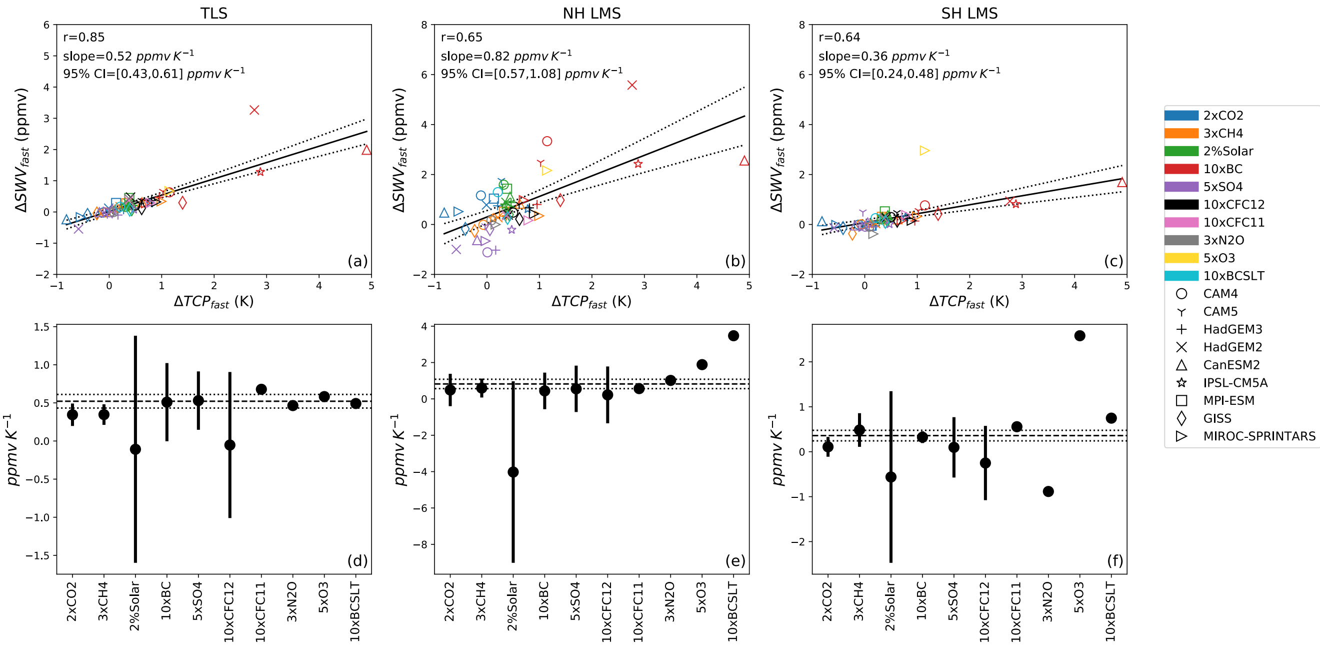

Figure 6. Panels (a)-(c): Linear regression between ΔSWV_{fast} (ppmv) and ΔTCP_{fast} (K) from all models and perturbations. The color coding indicates different perturbations, while the marker shapes indicate results from different models. The black solid line is the linear fit of the regression. The black dotted lines indicate the linear fits within the 95% confidence interval, estimated using a t-test. Panels (d)-(f): Slopes and their 95% confidence intervals obtained from linear regression between ΔSWV_{fast} (ppmv) and ΔTCP_{fast} (K) for each individual perturbation. The black dashed lines and dotted lines are the slopes and their 95% confidence intervals of regressions in (a)-(c).